ChemComm

COMMUNICATION

View Article Online
View Journal | View Issue

Cite this: *Chem. Commun.*, 2022, **58**, 10548

Received 18th July 2022,
Accepted 11th August 2022

DOI: 10.1039/d2cc03996f

rsc.li/chemcomm

Stern–Volmer analysis of photocatalyst fluorescence quenching within hollow-core photonic crystal fibre microreactors†

Alexander S. Gentleman, ‡[ab] Takashi Lawson, ‡[ab] Matthew G. Ellis,[a] Molly Davis,[a] Jacob Turner-Dore,[c] Alison S. H. Ryder,[c] Michael H. Frosz,[d] Maria Ciaccia,[e] Erwin Reisner,[b] Alexander J. Cresswell*[c] and Tijmen G. Euser*[a]

We report the use of optofluidic hollow-core photonic crystal fibres as microreactors for Stern–Volmer (SV) luminescence quenching analysis of visible-light photocatalytic reactions. This technology enables measurements on nanolitre volumes and paves the way for automated SV analyses in continuous flow that minimise catalyst and reagent usage. The method is showcased using a recently developed photoredox-catalysed α-C–H alkylation reaction of unprotected primary alkylamines.

Photocatalysis is of pivotal significance in two critical fields of human endeavour: the conversion of solar energy (sunlight) into small molecule feedstocks or fuels (*e.g.*, H_2, CO, CH_4),[1,2] and the chemical synthesis of complex organic molecules such as pharmaceuticals and crop protection agents.[3,4] Regardless of the application, it is important to attain an enhanced understanding of the mechanisms underlying photocatalytic reactions by providing experimental data for their verification.[5] A factor of central mechanistic importance in photocatalysis is the kinetic partitioning of the catalyst's excited state, PC*, between productive quenching (which leads to the chemical reaction of interest) *versus* non-productive relaxation. The relaxation of PC* can be either radiative (*i.e.*, fluorescence from ^{1}PC* or phosphorescence from ^{3}PC*), or it can be non-radiative (*e.g.*, $S_1 \rightarrow S_0$ internal conversion followed by vibrational relaxation), transferring thermal energy to the bulk medium in the latter case. These energy dispersal mechanisms have profound implications not only for the quantum efficiency of the catalysis – clearly of paramount importance for energy storage applications – but also for the catalytic turnover rate of the reaction.[6] The fractionation between quenching and relaxation for a given photocatalyst-quencher combination is used for mechanistic interrogation in photocatalytic reaction development to identify or confirm which molecular species is engaging with the excited photocatalyst. A common technique is luminescence quenching (Stern–Volmer) analysis, which measures the rate of quenching of PC* by a given quencher species, as a function of its concentration, in competition with radiative decay processes.[7] In fact, this technique has found application beyond the provision of mechanistic insight and has recently been leveraged as a high-throughput screening technology for the discovery of novel synthetic organic transformations.[8,9]

We have previously shown that energy dispersal mechanisms in photocatalytic reactions can be studied within liquid-filled hollow-core photonic crystal fibres (HC-PCFs):[10,11] a novel class of optofluidic waveguides that allow light to be guided at the centre of a microfluidic channel.[12,13] By infiltrating chemicals and monitoring their spectra (fluorescence, absorption, infrared, and/or Raman), reaction dynamics and steady-state concentrations can be probed *in situ*.[14–21] Major advantages of these new 'optofluidic microreactors' over conventional sample cells are the enhanced detection sensitivity (from meter-scale optical-paths), tiny sample volumes of a few nL per cm fibre length (*i.e.*, five orders of magnitude less than in conventional sample cells) and well-defined light-matter interactions: all key for the quantitative analysis of photochemistry.[14–21] As such, they provide an ideal way to gain insight into the energy dispersal mechanisms of PCs under reaction conditions.

We introduce a new fibre-based, optofluidic microreactor approach to perform Stern–Volmer fluorescence quenching analysis on homogeneous photocatalytic reactions on a nanolitre scale.[22–24] The principal motivation is to reduce by several

[a] *Nanophotonics Centre, The Cavendish Laboratory, University of Cambridge, JJ Thomson Avenue, Cambridge, CB3 0HE, UK. E-mail: te287@cam.ac.uk*
[b] *Yusuf Hamied Department of Chemistry, University of Cambridge, Lensfield Road, Cambridge, CB2 1EW, UK*
[c] *Department of Chemistry, University of Bath, 1 South, Claverton Down, Bath, BA2 7AY, UK*
[d] *Max Planck Institute for the Science of Light, Staudtstr. 2, 91058, Erlangen, Germany*
[e] *Syngenta, Jealott's Hill Research Centre, Bracknell, Berkshire, RG52 6EY, UK*

† Electronic supplementary information (ESI) available. See DOI: https://doi.org/10.1039/d2cc03996f

‡ These authors contributed equally to this work.

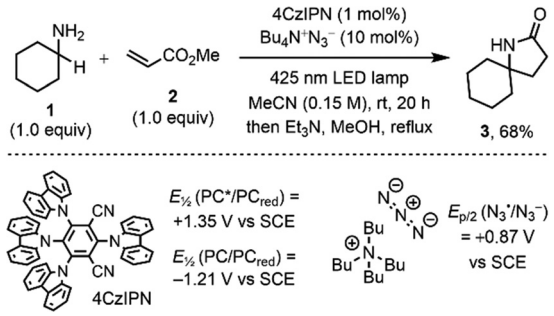

Fig. 1 Scope for the photocatalytic α-C–H alkylation of unprotected amines, *e.g.* cyclohexylamine (**1**)) with methyl acrylate (**2**) to synthesise γ-lactams (**3**) using the 4CzIPN photocatalyst.

orders of magnitude the quantities of catalysts and reagents necessary to perform such measurements by comparison to cuvette-based protocols. Ultimately, the longer-term objective is to design a fully-automated, high-throughput screening platform – based on HC-PCFs – to optimise or discover new photocatalysts or novel photocatalytic reactions.

As a proof-of-concept, we interrogate and verify the mechanism of a visible-light photoredox reaction recently developed by us for the α-C–H alkylation of unprotected primary amines (*e.g.*, **1**) with methyl acrylate **2** to access γ-lactams (*e.g.*, **3**) (Fig. 1).[25] This transformation deploys the organophotocatalyst 2,4,5,6-tetra(9*H*-carbazol-9-yl)isophthalonitrile (4CzIPN) in union with an azide ion (N_3^-) as a hydrogen atom transfer (HAT) co-catalyst.[26,27] The azide is introduced as tetrabutylammonium azide (Bu_4NN_3), which affords solubility in acetonitrile (MeCN).

We have previously utilised cuvette-based Stern–Volmer analyses to ascertain that the azide ion (N_3^-) co-catalyst serves as the primary reductive quencher for [4CzIPN]*, albeit with some very minor competitive quenching by the primary amine substrate (*e.g.*, **1**). Thus, we elected to reinvestigate the same reaction *via* Stern–Volmer fluorescence quenching analysis in an HC-PCF, to provide a head-to-head comparison with cuvette-based analysis for this system. Agreement with the former measurements would provide confidence that our HC-PCF approach provides robust and accurate experimental data, and would provide a pretext for its future use in the analysis of other photocatalytic processes.

For the in-fibre investigation of the fluorescence quenching dynamics of 4CzIPN, we employed a kagomé-style HC-PCF, a PCF type first used by Benabid *et al.*[28] The kagomé-style HC-PCF implemented here was fabricated with a core diameter and wall thickness of 30 μm and 160 nm, respectively (Fig. 2a–c inset). This design allows for excellent guidance across the entire visible wavelength range when infiltrated with acetonitrile, as confirmed experimentally (Fig. S4, ESI†).

A 20 cm length of kagomé HC-PCF was connected to liquid cells, and infiltrated with a sample solution using a standard syringe pump and PEEK tubing. A 5 cm long fibre section was side-irradiated with a diffuse LED source (Fig. S1, ESI†) in order to ensure homogenous irradiation of the infiltrated sample. This method of excitation allows for the fluorescence to be collected more efficiently over a longer fibre length than *via*

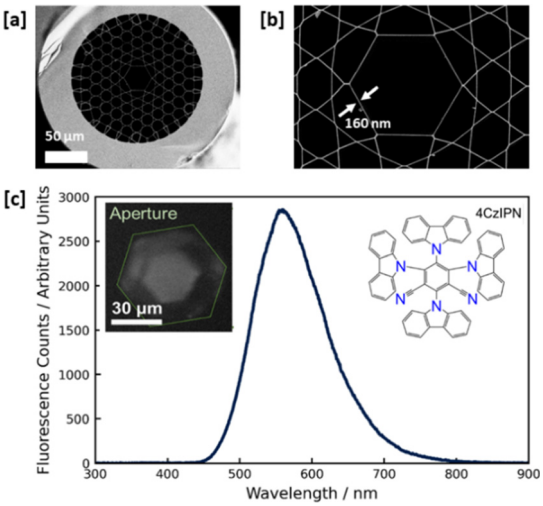

Fig. 2 Dimensions and fluorescence transmission properties of the kagomé-style hollow-core photonic crystal fibre (HC-PCF). (a) Scanning electron microscope (SEM) image of the kagomé-style HC-PCF; (b) close-up SEM image of the fibre core with the inner strut thickness; (c) measured in-fibre fluorescence spectrum of the 4CzIPN photocatalyst (λ_{exc} = 365 nm). Inset: Camera image of 4CzIPN fluorescence emanating from the core region spatially selected using aperture A1 in Fig. S1a (ESI†) (green hexagon).

in-coupling of the pump light as the excitation power becomes dependent on the sample concentration for the latter method (especially in cases where the quencher absorbance is high), thus confining any fluorescence emanating from the core to the first few centimetres of fibre.

Even though side-irradiation will result in excitation of the solution in the fibre cladding as well as the hollow core, the fluorescence signal emerging from the fibre core was spatially filtered and divided between a camera and spectrometer, ensuring that only core fluorescence is being monitored. The coupling to the spectrometer (Ocean Optics QE65000) was done through a multimode fibre with a 100 μm core diameter (see Fig. S1, ESI†). The fluorescence spectrum of 4CzIPN measured from this kagomé HC-PCF (Fig. 2c) compares well with that recorded using a commercial fluorometer from almost 21 500 times a larger sample volume within a conventional cuvette (see Fig. S2, ESI†), displaying similar fluorescence maxima at 546 nm (cuvette) and 558 nm (HC-PCF) in acetonitrile (Fig. 2c and Fig. S2, ESI†). As the comparison between the fluorescence spectra from both the cuvette and fibre is favourable, any difference in fluorescence resulting from surface-adsorbed molecules on the wall of the fibre core must be minute in comparison to that from free fluorescent molecules in the fibre core.

In-fibre Stern–Volmer analysis was first conducted with tetrabutylammonium azide (Bu_4NN_3) to determine the rate at which it can quench the excited state of 4CzIPN, with the results presented in Fig. 3. A background ('control') fluorescence spectrum taken prior to loading with 4CzIPN samples shows that the background fluorescence from the HC-PCF infiltrated with pure acetonitrile was negligible (Fig. 3a). Stern–Volmer analysis is performed by fitting the normalised

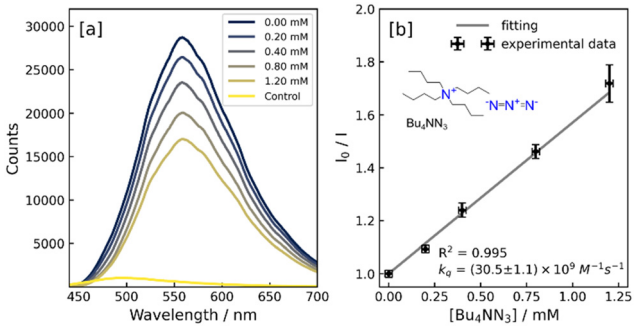

Fig. 3 Fluorescence quenching of 30 μM 4CzIPN by tetrabutylammonium azide (Bu_4NN_3). Fluorescence profiles at each quencher concentration are shown in (a), with a Stern–Volmer plot presented in (b). A control measurement in (a) confirms that fluorescence from the HC-PCF is insignificant compared to 4CzIPN. Error bars in (b) correspond to the standard error of triplicates.

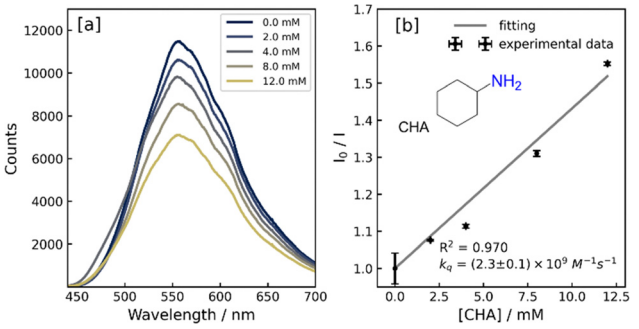

Fig. 4 Fluorescence quenching of 30 μM 4CzIPN by cyclohexylamine (CHA). Fluorescence profiles at each quencher concentration are shown in (a), with a Stern–Volmer plot presented in (b). Error bars in (b) correspond to the standard error of triplicates.

integrated counts (I_0/I_n) to the linear function in eqn (1). Here, plotting I_0/I_n *vs.* quencher concentration ($[Q]_n$) whilst accounting for the fluorescence lifetime in the absence of a quencher, τ_0 = 18.7 ns (inverse of the rate constant associated with the prompt fluorescence recorded from the 365 nm excitation of 4CzIPN in acetonitrile),[29] gives a Stern–Volmer bimolecular quenching rate constant, k_a, of (30.5 ± 1.1) × 10^9 L mol^{-1} s^{-1} with strong confidence (R^2 = 0.995).

Fluorometer-based measurements (see Fig. S6, ESI†) with the same data analysis methodology and triplicate repeats gave a similar k_q of (26.2 ± 2.0) × 10^9 L mol^{-1} s^{-1} with a slightly lower confidence R^2 = 0.929, showing the reproducibility of our Stern–Volmer measurements between separate measurement platforms. In addition, fibre-based measurements enabled a bimolecular rate constant to be extracted on a 10^4 times smaller sample volume than fluorometer-based measurements (140 nL compared to 2 mL per measurement – Fig. S6, ESI†).

$$\frac{I_0}{I_n} = 1 + k_q\tau_0[Q] \quad (1)$$

Fluorescence reabsorption by CHA or Bu_4NN_3 quenchers is expected to be negligible due to the marginal overlap between absorbance (Fig. S3, ESI†) and 4CzIPN fluorescence profiles (Fig. S2, ESI†). However, over the 10 cm propagation from the excitation region to the fibre end, residual quencher reabsorption may become noticeable due to the longer optical path length. The 4CzIPN spectrum at the highest concentration of the most absorbing quencher (1.2 mM Bu_4NN_3) shows a reduction of collected photons (*ca.* 4%) at the short-wavelength side of the spectrum compared to a sample without Bu_4NN_3. This shows that the effects of quencher reabsorption on the Stern–Volmer analysis are minimal (Fig. S7, ESI†). The small redshift of *ca.* 12 nm in the quencher-free fibre fluorescence spectrum (Fig. S2, ESI†), may be related to slight differences in the wavelength-response of the two spectrometers and/or residual reabsorption by 4CzIPN. However, this does not affect the Stern–Volmer analysis, as it is based on the relative reduction of total counts.

A similar in-fibre Stern–Volmer analysis was conducted with cyclohexylamine (**1**, CHA) to compare against Bu_4NN_3 (Fig. 4). We find that CHA as a quencher for 4CzIPN is less effective and report a bimolecular quenching rate constant, k_q, of (2.3 ± 0.1) × 10^9 L mol^{-1} s^{-1} with moderate confidence (R^2 = 0.970). Fluorometer-based measurements (see Fig. S8, ESI†) with the same data analysis methodology and triplicate repeats gave a similar k_q of (2.2 ± 0.1) × 10^9 L mol^{-1} s^{-1} with a similar confidence R^2 = 0.979.

To give a clearer interpretation of the azide anion and cyclohexylamine **1** as quenchers, the proportion of excited states interacting with each quencher (F_q) is calculated from the fluorescence lifetime (τ_0) and bimolecular quenching rate constant, as shown in eqn (2). We observe that 36% of the exited state of 4CzIPN is quenched by 1 mM of azide compared to 4% with 1 mM of CHA.

$$F_q = \frac{k_q[Q]}{(1/\tau_0) + k_q[Q]} \quad (2)$$

From our in-fibre Stern–Volmer analysis (Fig. 3b and 4b), the Bu_4NN_3 is shown to be much more efficient than CHA **1** at quenching the excited state of 4CzIPN, with k_q values comparing very favourably to those derived from our cuvette-based measurements. These results are also consistent with previous observations by Cresswell *et al.*, despite the k_q values derived from their reported K_{SV} values being at least an order of magnitude different due to systematic errors associated with the removal of oxygen contamination prior to fluorescence analysis (k_q = 14.0 × 10^{10} M^{-1} s^{-1} and 6.69 × 10^8 M^{-1} s^{-1} for Bu_4NN_3 and CHA fluorescence quenchers, respectively).[30] Even though the bimolecular quenching rate coefficient obtained for Bu_4NN_3 is of a similar magnitude to the rate of diffusion (k_{diff} ~ 10^{10} s^{-1}),[31] our in-fibre Stern–Volmer analysis cannot distinguish between static and dynamic (collisional) quenching pathways and, as such, further experimentation is necessary for deeper understanding (*e.g.*, excited-state lifetime studies). However, the comparison of k_q values for Bu_4NN_3, and CHA **1** clearly affirms our previous assignment[25] of the azide ion, N_3^-, as the primary reductive quencher of 4CzIPN* in the photoredox process. Single electron transfer (SET) is strongly implicated,

based on EPR detection of spin-trapped $N_3^\bullet$ in studies of N_3^- oxidation by photoexcited 4CzIPN,[32] as well as redox potentials w.r.t. SCE in MeCN ($E_{p/2}$ of N_3^- = +0.87 V; $E_{p/2}$ of CHA = +1.53 V; $E_{1/2}$ (4CzIPN*/4CzIPN$^{\bullet-}$) = +1.35 V).[25,33] In the proposed mechanism (Fig. S9, ESI†), subsequent HAT from the relatively weak α-C–H bond of CHA **1** (BDE = 89–91 ± 2 kcal mol^{-1})[34] by $N_3^\bullet$ occurs to give α-amino radical (**4** – Fig. S9, ESI†), which undergoes addition to the acrylate acceptor **2** to give an α-carboxy radical (**5** – Fig. S9, ESI†) [$E_{1/2} \sim -0.63$ V *vs.* SCE[35]]. Reduction of this radical to the corresponding enolate (**6** – Fig. S9, ESI†) by the [4CzIPN]$^{\bullet-}$ radical anion [$E_{\frac{1}{2}}$ (PC/PC$^{-\bullet}$) = −1.21 V *vs.* SCE in MeCN] is presumably followed by proton transfer from HN_3 (pK_a = 7.9 in DMSO) to give the γ-amino ester product (**7** – Fig. S9, ESI†) and regenerate the azide ion. A subsequent lactamisation step then converts **7** to γ-lactam **3**.

In summary, we have shown that quantitative fluorescence spectroscopy can be performed on 140 nL volumes using optofluidic hollow-core photonic crystal fibre microreactors. PCF-microreactor Stern–Volmer analysis was successfully exemplified on a visible-light photoredox catalysed reaction using a widely used organophotocatalyst (4CzIPN). The resulting bimolecular quenching rate constant for [4CzIPN*] with N_3^- ion and with cyclohexylamine **1** were comparable to conventional fluorometer methods, despite the 10^4 times reduction in sample volume. This work provides a firm foundation for automated fluorescence screening of photoredox catalysts with quencher concentrations adjusted in continuous flow, while minimising the consumption of precious and expensive reagents.

T. G. E., E. R., and A. S. G. thank the Leverhulme Trust (RPG-2018-256), the Winton Programme for the Physics of Sustainability, and the Isaac Newton Trust. T. L. acknowledges the Cambridge NanoDTC (EPSRC Grant EP/L015978/1). A. J. C. thanks the Royal Society for a URF (UF150533), and the EPSRC and Syngenta for an iCASE PhD studentship (J. C. T.-D.).

Conflicts of interest

The authors have no conflict of interest to declare.

Notes and references

1 G. A. M. Hutton, B. C. M. Martindale and E. Reisner, *Chem. Soc. Rev.*, 2017, **46**, 6111–6123.
2 A. Bachmeier, B. Siritanaratkul and F. A. Armstrong, in *From Molecules to Materials*, ed. E. A. Rozhkova and K. Ariga, Springer Intern. Publishing, Cham, 2015, pp. 99–123.
3 V. Balzani, G. Bergamini and P. Ceroni, *Rend. Lincei*, 2016, **28**, 125–142.
4 C. R. J. Stephenson, T. P. Yoon and D. W. C. MacMillan, *Visible light photocatalysis in organic chemistry*, Wiley-VCH Verlag, 2018.
5 T. Noël and E. Zysman-Colman, *Chem. Catal.*, 2022, **2**, 468–476.
6 J. Z. Bloh, *Front. Chem.*, 2019, **7**, 128.
7 J. R. Lakowicz, *Principles of Fluorescence Spectroscopy*, Springer-Verlag, New York, 2006.
8 F. Strieth-Kalthoff, C. Henkel, M. Teders, A. Kahnt, W. Knolle, A. Gómez-Suárez, K. Dirian, W. Alex, K. Bergander, C. G. Daniliuc, B. Abel, D. M. Guldi and F. Glorius, *Chem*, 2019, **5**, 2183–2194.
9 M. N. Hopkinson, A. Gómez-Suárez, M. Teders, B. Sahoo and F. Glorius, *Angew. Chem., Int. Ed.*, 2016, **55**, 4361–4366.
10 A. M. Cubillas, S. Unterkofler, T. G. Euser, B. J. M. Etzold, A. C. Jones, P. J. Sadler, P. Wasserscheid and P. S. J. Russell, *Chem. Soc. Rev.*, 2013, **42**, 8629–8648.
11 M. Schmidt, A. M. Cubillas, N. Taccardi, T. G. Euser, T. Cremer, F. Maier, H.-P. Steinrück, P. S. J. Russell, P. Wasserscheid and B. J. M. Etzold, *ChemCatChem*, 2013, **5**, 641–650.
12 P. Russell, *Science*, 2003, **299**, 358–362.
13 G. Antonopoulos, F. Benabid, T. A. Birks, D. M. Bird, J. C. Knight, P. J. Russell, R. F. Cregan, B. J. Mangan, P. J. Roberts and D. C. Allan, *Opt. Express*, 2006, **14**, 3000–3006.
14 P. Koehler, T. Lawson, J. Neises, J. Willkomm, B. C. M. Martindale, G. A. M. Hutton, D. Antón-García, A. Lage, A. S. Gentleman, M. H. Frosz, P. S. J. Russell, E. Reisner and T. G. Euser, *Anal. Chem.*, 2021, **93**, 895–901.
15 A. S. Gentleman, E. Miele, T. Lawson, P. Köhler, S. Kim, S. Yousaf, D. A. Garcia, A. Lage, C. P. Grey, J. J. J. Baumberg, M. H. Frosz, P. S. J. Russell, E. Reisner and T. G. Euser, in 14th Pacific Rim Conference on Lasers and Electro-Optics (CLEO PR 2020), OSA, Washington, DC, 2020.
16 G. O. S. Williams, T. G. Euser, J. Arlt, P. S. J. Russell and A. C. Jones, *ACS Photonics*, 2014, **1**, 790–793.
17 G. O. S. Williams, T. G. Euser, P. S. J. Russell and A. C. Jones, *Methods Appl. Fluoresc.*, 2013, **1**, 015003.
18 S. Smolka, M. Barth and O. Benson, *Opt. Express*, 2007, **15**, 12783.
19 G. O. S. Williams, T. G. Euser, P. S. J. Russell, A. J. MacRobert and A. C. Jones, *ChemPhotoChem*, 2018, **2**, 616–621.
20 D. Yan, J. Popp, M. W. Pletz and T. Frosch, *ACS Photonics*, 2017, **4**, 138–145.
21 F. Schorn, M. Aubermann, R. Zeltner, M. Haumann and N. Y. Joly, *ACS Catal.*, 2021, **11**, 6709–6714.
22 M. H. Gehlen, *J. Photochem. Photobiol., C*, 2020, **42**, 100338.
23 K. P. L. Kuijpers, C. Bottecchia, D. Cambié, K. Drummen, N. J. König and T. Noël, *Angew. Chem., Int. Ed.*, 2018, **57**, 11278–11282.
24 S. Bold, L. Zedler, Y. Zhang, J. Massin, V. Artero, M. Chavarot-Kerlidou and B. Dietzek, *Chem. Commun.*, 2018, **54**, 10594–10597.
25 A. S. H. Ryder, W. B. Cunningham, G. Ballantyne, T. Mules, A. G. Kinsella, J. Turner-Dore, C. M. Alder, L. J. Edwards, B. S. J. McKay, M. N. Grayson and A. J. Cresswell, *Angew. Chem., Int. Ed.*, 2020, **59**, 14986–14991.
26 H. E. Askey, J. D. Grayson, J. D. Tibbetts, J. C. Turner-Dore, J. M. Holmes, G. Kociok-Kohn, G. L. Wrigley and A. J. Cresswell, *J. Am. Chem. Soc.*, 2021, **143**(39), 15936–15945.
27 J. D. Grayson and A. J. Cresswell, *Tetrahedron*, 2021, **81**, 131896.
28 F. Benabid, J. C. Knight, G. Antonopoulos and P. S. J. Russell, *Science*, 2002, **298**, 399–402.
29 R. Ishimatsu, S. Matsunami, K. Shizu, C. Adachi, K. Nakano and T. Imato, *J. Phys. Chem. A*, 2013, **117**, 5607–5612.
30 A. S. H. Ryder, W. B. Cunningham, G. Ballantyne, T. Mules, A. G. Kinsella, J. Turner-Dore, C. M. Alder, L. J. Edwards, B. S. J. McKay, M. N. Grayson and A. J. Cresswell, *Angew. Chem., Int. Ed.*, 2020, **59**, 14986–14991.
31 N. A. Romero and D. A. Nicewicz, *Chem. Rev.*, 2016, **116**, 10075–10166.
32 M. Shee, S. S. Shah and N. D. P. Singh, *Chem. – Eur. J.*, 2020, **26**, 14070–14074.
33 J. Luo and J. Zhang, *ACS Catal.*, 2016, **6**, 873–877.
34 Y. R. Luo, *Comprehensive Handbook of Chemical Bond Energies*, CRC Press, Boca Ratan, FL, 2007.
35 N. Bortolamei, A. A. Isse and A. Gennaro, *Electrochim. Acta*, 2010, **55**, 8312–8318.